

Effect of Succinonitrile on Ion Transport in PEO-based Lithium Ion Battery Electrolytes

Sipra Mohapatra^{1,†}, Shubham Sharma^{1,†}, Aman Sriperumbuduru¹, Srinivasa Rao Varanasi², and Santosh Mogurampelly^{1,*}

¹Department of Physics, Indian Institute of Technology Jodhpur, Karwar, Rajasthan 342027, India

²Department of Physics, Sultan Qaboos University, Al-Khoud 123, Muscat, Oman.

ABSTRACT:

We report the ion transport mechanisms in succinonitrile (SN) loaded solid polymer electrolytes containing polyethylene oxide (PEO) and dissolved lithium bis(trifluoromethane)sulphonamide (LiTFSI) salt using molecular dynamics simulations. We investigated the effect of temperature and loading of SN on ion transport and relaxation phenomenon in PEO-LiTFSI electrolytes and observed that SN increases the ionic diffusivities in PEO-based solid polymer electrolytes and makes them suitable for battery applications. Interestingly, the diffusion coefficient of TFSI ions was found to be an order of magnitude higher than the diffusion coefficient of lithium ions across the range of temperatures and loadings integrated. By analyzing different relaxation timescales and examining the underlying transport mechanisms in SN-loaded systems, we find that the diffusivity of TFSI ions correlates excellently with the Li-TFSI ion-pair relaxation timescales. In contrast, our simulations predict distinct transport mechanisms for Li-ions in SN-loaded PEO-LiTFSI electrolytes. Explicitly, the diffusivity of lithium ions cannot be uniquely determined by the ion-pair relaxation timescales but additionally depends on the polymer segmental dynamics. On the other hand, the SN loading induced diffusion coefficient at a given temperature does not correlate with either the ion-pair relaxation timescales or the polymer segmental relaxation timescales.

*address for correspondence: santosh@iitj.ac.in

[†]equal first author contribution

1. INTRODUCTION

The growing demand for new generation portable electronic devices is driving the technological development of rechargeable solid-state batteries. The Li ion batteries offer many interesting properties such as high energy density, lightweight, flexible, and longevity among many other properties.¹⁻³ Solid polymer electrolytes (SPEs) are becoming increasingly attractive electrolyte materials for lithium ion batteries because of their safety, flexibility, and mechanical strength.⁴⁻⁶ They also have good electrochemical stability, low flammability, and toxicity with the ability to form good interfacial materials with the electrodes thereby eliminating the need for a separator. Polyethylene oxide (PEO) is a promising candidate for SPE applications in Li ion batteries. However, they possess a very low ionic conductivity (in a range of 10^{-8} to 10^{-4} S/cm at room temperature) as compared to liquid electrolytes which makes them less practical for commercial applications.^{7,8} Therefore, there is a quest for new generation electrolyte designs offering increase ionic conductivity of PEO-based SPEs. In this context, we hypothesize that a thorough understanding of the fundamental transport mechanisms is necessary to provide guidelines on design strategies for new generation electrolytes.

The PEO is a semi-crystalline polymer with a chemical structure of $\text{H}-(\text{O}-\text{CH}_2-\text{CH}_2)_n-\text{OH}$. The ether oxygens (EO) units in PEO acts as a promising association site for Li ions which makes the PEO a promising ion-solvating candidate for promoting faster ion transport for the battery applications. A study by Fenton et al. in 1973 found that alkali metals get easily dissolved in PEO to form conductive complexes.⁹ In 1975 Peter V. Wright, a polymer chemist from Sheffield, first found PEO as a host for sodium and potassium salts for solid-based electrical conductor polymer-salt complex.^{10,11} A mechanistic study by Michel Armand established in 1983 that the ionic motion is due to the amorphous region in polymer-salt complexes.¹² Soon after that, explaining the physics of PEO became an active research area to understand its ion transport mechanism, chemical and physical properties at the electrode/electrolyte interface.²

The ion transport mechanism of neat amorphous PEO melt has been previously using both experimentally and theoretically.¹³⁻¹⁶ It was reported that the amorphous phase of PEO activates the chain segments which aids the ion transport whereas its crystalline phase slows down the polymer chain dynamics.¹⁴ In SPEs, the Li ions are located at specific coordinate sites near the EO groups in polyethylene oxide chains which undergo a constant segmental motion. As a result, the lithium ion hops from one EO site to the other along the backbone of the polymeric chain and intermittently jumps from one chain to another under the motion of segmental motion of polymeric chains. Borodin and Smith in PEO-based SPEs studied the ion transport mechanism in amorphous PEO/LiTFSI and

observed the diffusion of Li and TFSI ions are strongly coupled to PEO ether oxygen atom displacement and its conformational dynamics.¹⁴

More importantly, traditional lithium salts (LiClO₄, LiPF₆, LiAsF₆, LiBF₄, etc.) are found to aggregate strongly in SPEs¹⁷ Ion aggregation, which depends on the size of anion, increases with salt concentration and temperature due to the delocalization of charge on large-sized anions.¹⁸ The bis(trifluoromethane)sulphonamide anion (TFSI⁻), class of ILs is a popular anion for Li ion battery applications because of its large size. Piotr et al. investigated the correlations in ion transport in LiTFSI electrolytes and found that irrespective of the type of cation, the motion of cation and anion (TFSI) are strongly correlated which in turn result in reduced ionic conductivity.¹⁹ In 2000, Borodin and Smith studied the dynamics of cation and anion in LiI-doped diglyme and poly(ethylene oxide) solutions having (EO: Li)=15:1 and 5:1¹³ and found that ion-aggregation is greater in the case of diglyme/LiI solution which results in a decrease of ion mobility and conductivity. Further, they also observed that EO-Li association lifetime is highly correlated with torsional autocorrelation time for -O-C-C-O-dihedrals.

To alleviate the problem of high crystallinity in neat SPEs, some solvents/plasticizers are typically added to the electrolyte which increases the amorphous nature of the polymer matrix.²⁰ Many experimentalists have studied the effect of adding different solvents to the PEO matrix on ionic conductivity. For instance, Ahn et al. incorporated 1-butyl-3-methylimidazolium-bis (trifluoromethane sulfonyl) imide (BMITFSI) in the PEO-LiTFSI complex, found that with the increase in BMITFSI content the ionic conductivity increases and the reported value is 0.32 mS/cm at room temperature.²¹ Several molecular dynamics studies also reported that the PEO matrix incorporated with different solvents shows better ionic conductivity and polymer flexibility.^{13,22–27}

Due to the presence of plasticity and a high degree of polarity, succinonitrile (SN) is seen as a potential additive in polymer electrolytes.^{1,28–31} Experimentalists have observed a high ionic conductivity (~0.35 mS/cm at 30°C), and high mechanical stability because of decrease in tensile strength in SPEs by appropriately optimising the content of SN and PEO.²⁸ It is demonstrated that different polymer electrolytes P(VDF-HFP)–LiTFSI and P(VDF-HFP)–LiBETI show excellent mechanical properties when SN is used as a dispersant.³¹ Gianni et al. have investigated the dynamical properties of succinonitrile by calculating the time dependency of single-molecule autocorrelation functions and found three distinct regimes of orientation relaxation.¹ Also, it is observed that the complex formed by PEO and alkali metal salts had shown fast alkali metal transport at 100°C.⁹ While a number of experimental studies have been carried out to understand the influence of SN on ionic conductivity in

a polymer matrix, a molecular-level understanding of the mechanisms of ion transport is not understood.^{28–31} Particularly, a fundamental understanding of the factors influencing ion transport in SN-loaded systems is lacking. Molecular dynamics with atomistic level resolution is a powerful tool to gain deeper physical insight into the ion-transport mechanisms. Therefore, we considered the atomistic molecular dynamics simulations comprising of PEO-LiTFSI matrix dispersed with succinonitrile (SN) molecules at the desired loading. Our primary motivation for this study is: (i) To examine the diffusivities of ions when SN is loaded in PEO-LiTFSI (ii) To understand the governing factor of ionic diffusivities through the ion-pair interactions and polymer segmental motion, and finally, (iii) Explaining the transport mechanisms of ions inside the PEO matrix solvated with Li-TFSI and SN molecules. Ion-pair relaxation times and dihedral relaxation times were calculated to understand the interplay of interactions of Li ion with its anionic pair (TFSI⁻) and polymer (PEO).^{13,14,16,23,32–36}

Towards the above-outlined objectives, we analysed the results of MD simulations of SN-PEO-LiTFSI by varying the temperature, and loading of SN. The effect of succinonitrile on ion transport mechanisms was investigated using fully atomistic simulations of 200 ns and longer depending on the loading and temperature. We have calculated the diffusion coefficients of both Li⁺ (cation) and TFSI⁻ (anion) at a concentration (EO: Li = 12.5:1) and different weight percentages of SN in PEO-LiTFSI melt. The temperature effects on ion transport were studied by performing simulations at different temperatures ranging between 375 K to 575 K. Together, our results indicate the SN-induced changes in ion-pair relaxations and polymer dynamics arising from ion-ion interactions and ion-polymer interactions, respectively are the main mechanisms of ion transport in SN-loaded PEO-LiTFSI electrolytes.

The organisation of the rest of the paper is as follows: In section **2**, we present the simulation details including the interaction potential field and force field parameters used, initial system setup, equilibration, and production protocols. In section **3.1**, we present the results diffusion coefficients calculated from mean-squared displacement (MSD) of Li and TFSI ions respectively. In section **3.2**, we identify different mechanisms influencing ion mobility. Explicitly, in section **3.2.1**, we present the results for ion-pair autocorrelation functions, corresponding relaxation times with diffusivities and discuss the correlations with ionic mobility. In section **3.2.2**, we present the results of dihedral autocorrelation functions, corresponding relaxation times and examine their connection with polymer segmental motion. Finally, in section **4**, we summarized our results and concluded essential findings of understanding the ion transport mechanisms in SN-PEO-LiTFSI electrolytes.

2. SIMULATION METHODS

2.1. Interaction Potential and Force Fields. We used atomistic molecular dynamics (MD) simulations to investigate the PEO-LiTFSI electrolytes loaded with SN molecules. The molecular dynamics simulations of SN-PEO-LiTFSI system were performed using GROMACS³⁷ (GRoningen MAchine for Chemical Simulation) package employing the following general form of interaction potential between different atoms:

$$U(r) = U^{\text{bonded}}(r) + \sum 4\epsilon_0 \left[\left(\frac{\sigma}{r_{ij}} \right)^{12} - \left(\frac{\sigma}{r_{ij}} \right)^6 \right] + \sum \frac{q_1 q_2}{4\pi\epsilon_0 r_{ij}} \quad (1)$$

where U^{bonded} describes the interactions arising from bonds, angles, and torsions in PEO. The bonded interactions in PEO were modelled with a harmonic potential $\frac{1}{2}k_r(r - r_0)^2$, the angles with $\frac{1}{2}k_\theta(\theta - \theta_0)^2$ and torsions with $\frac{1}{2}\sum_{n=1}^4 C_n [1 + (-1)^{n+1}\cos(n\phi)]$. The non-bonded interactions are modelled with the Lennard-Jones potential and the Coulombic electrostatic potential. The parameters in eq 1 are obtained from the set of Optimized Potentials for Liquid Simulations (OPLS) forcefield.^{38,39} A scaling factor of 0.5 was used to calculate the effective nonbonded interactions associated with intramolecular atomic pairs separated by three bonds and complete nonbonded interactions are considered for intramolecular atomic pairs beyond three bonds. The nonbonded parameters for cross-interaction terms between different atomic types were estimated using the Lorentz-Berthelot mixing rules.

The total charge on ionic species was scaled to 0.8e to indirectly mimic the induced polarization effects in a mean field like manner. Such an approach was previously shown to produce results in comparison with polarizable models and experiments.^{34,40-42} The charge scaling approach is being routinely employed in atomistic MD simulations as an alternate approach to reproduce the dynamics of ionic species in comparison with experiments.^{32,34,43-45} The partial charges of different atoms in our simulations are shown in Table 1.

Table 1. Partial charges on atom types used in our MD simulations

Atom (PEO)	q (e)	Atom (TFSI)	q (e)	Atom (SN)	q (e)
O	-0.40	F1	-0.128	C00	0.116
C	0.14	CBT	0.280	C01	-0.070
H	0.03	SBT	0.816	C02	-0.070
C1	0.11	OBT	-0.424	H03	0.144
Li	0.800	NBT	-0.528	H04	0.144

			C05	0.116
			H06	0.144
			H07	0.144
			N08	-0.335
			N09	-0.335

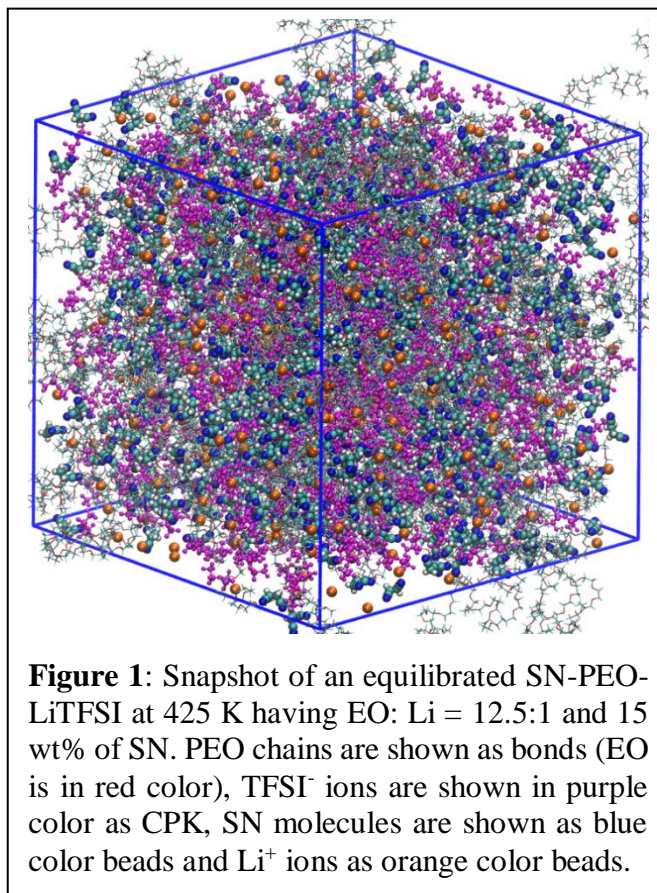
2.2. Initial System Setup. The initial conformation of PEO was constructed as follows: We built a single polymeric chain of 50 repeating monomeric units with chemical structure H-[CH₂-O-CH₂]₅₀-H corresponding to a molecular weight of 2.2 kD. Minimization was performed on this single PEO chain to get the desired bond lengths, angles, and torsion angles defined according to OPLS-AA force field parameters.^{38,39} The minimized configuration of a single PEO chain was then inserted randomly in a simulation box to generate a less dense system consisting of 100 chains of PEO using Packmol software.^{46,47} Then the system with pure 100 chains of PEO was solvated with appropriate numbers of Li⁺ cations and TFSI⁻ anions corresponding to a salt concentration of EO: Li=12.5:1 by placing the ions randomly into the simulation box.

The succinonitrile (SN) plasticisers were then dispersed randomly in the bulk PEO-LiTFSI matrix at different loadings of 0, 2.2, 10, 15, 20 wt% to build the complete system. The chemical structure of SN is [CN-CH₂-CH₂-CN] and has a molecular weight of 80.09 g/mol. It is a highly flexible solid plasticizer with a plastic crystalline organic molecular structure, stable between 233 and 331 K.¹ The density of the system in the initial stage was chosen as low as needed in order to easily solvate the Li⁺, TFSI⁻ and SN molecules in the PEO matrix. Such low density was chosen to ensure that the PEO melt does not suffer potential energy trap arising due to the contact with other molecules. The number of particles in each loaded system is shown in Table 2.

Table 2. Number of atoms for each loaded electrolyte system in our simulations

wt% of SN	Compositional Details				Total number of atoms
	# PEO Chains	# Li	# TFSI molecules	# SN molecules	
0	100	400	400	0	41600
2.2				100	42600
10				465	46250
15				740	49000
20				1050	52100

2.3. Equilibration Protocol. The complete SN-PEO-LiTFSI electrolyte systems containing appropriate proportions of polymers, ions, and plasticiser at each loading of SN were subjected to an equilibration procedure described previously.^{32,43} The initially built systems were minimized using the steepest descent method with a step size of 0.01 nm and the minimization treated as converged when the maximum force is smaller than 10 kJ mol⁻¹ nm⁻¹. The minimized structures were then subjected to a short NVT ensemble for 50 ps at 425 K using Berendsen thermostat⁴⁸ with a coupling constant of 1 ps. Further, a 10 ns NPT simulation was carried to bring out the low dense system to experimentally comparable dense state point. During this NPT stage, the system was coupled to a thermostat using the Nosé-Hoover algorithm⁴⁹⁻⁵¹ with a damping relaxation time of 1 ps and Parrinello-Rahman barostat⁵² with a damping relaxation time of 2 ps. The temperature was annealed to required values for systems having different wt%s of SN. The above-described protocol ensured appropriate equilibration of the electrolyte systems at the desired state point before long production runs of lengths 250 ns. The equations of motion were integrated using the leapfrog algorithm, and the trajectories were saved every 1 ps. We ran ten parallel runs with a saving frequency of 10 fs to analyse dihedral autocorrelation functions. Figure 1 displays a snapshot of equilibrated SPE of EO: Li = 12.5:1 and 15 wt % of SN containing PEO chains, Li⁺, TFSI⁻ and SN molecules.



The cut-off for LJ interactions was taken as 1.2 nm and the electrostatic interactions were calculated using the particle mesh Ewald (PME) method.⁵³ Periodic boundary conditions were applied in all the three directions. A brief summary of the simulation setup and equilibration densities is provided in Table 3. The densities obtained from the simulations are in good agreement with experimental densities. Furthermore, a small change in density is observed when adding SN with different loadings compared to SN-free electrolytes.

Table 3. A summary of the simulation setup and average density in the units of g/cm³. The values shown in parenthesis are the standard deviation on the average density.

EO: Li	T (K)	0 wt%	2.2 wt%	10 wt%	15 wt%	20 wt%
12.5:1	375	1.294(4)	1.282(4)	-	1.215(4)	-
	400	1.271(4)	1.259(4)	-	-	-
	425	1.249(4)	1.236(4)	1.195(4)	1.168(4)	1.143(4)
	450	1.227(4)	1.214(4)	-	-	-
	475	1.206(4)	1.193(5)	-	1.123(5)	-
	500	1.184(5)	1.171(5)	-	-	-
	525	1.163(5)	1.150(5)	-	1.078(5)	-
	550	1.143(5)	1.129(5)	-	-	-
	575	1.122(6)	1.108(6)	-	1.033(6)	-

3. RESULTS AND DISCUSSION

3.1. Mean-Squared Displacement and Diffusion Coefficient. Following the equilibration protocol described above, we performed the molecular dynamics simulations at 1 bar pressure for temperature ranging from 375 K to 575 K at different loading of 0, 2.2, and 15 wt% of SN molecules. Moreover, we also performed MD simulations at 425 K with varied loadings of SN in PEO-LiTFSI electrolyte to understand the loading effect of SN on the ion transport. The transport characteristics of Li and TFSI ions were then studied by calculating the mean-squared displacement using $MSD(t) = \langle (\vec{R}(t) - \vec{R}(0))^2 \rangle$ where $\vec{R}(t)$ denotes the position vector of ions at a specific time t and $\langle \dots \rangle$ represents the ensemble average over number of particles and all possible time origins. The MSDs for different systems at different wt% and temperatures are presented in the supplementary information (SI).

The self-diffusion coefficient was then calculated using the Einstein's relation,

$$D = \lim_{t \rightarrow \infty} D^{\text{app}}(t) = \lim_{t \rightarrow \infty} \frac{\langle MSD(t) \rangle}{6t}, \quad (2)$$

where, $D^{\text{app}}(t)$ is the time-dependent apparent diffusion coefficient. We note that the MSDs were calculated from long enough trajectories to reach the diffusive regimes. The exponents, β on $MSD \sim t^\beta$ are shown in the SI. As we know, the Einstein relation holds true only for longer timescales in the diffusive regime at timescales ideally as $t \rightarrow \infty$. We calculated the standard deviation on the diffusion coefficient by dividing the diffusive part of the MSD curve into several blocks of equal sizes.

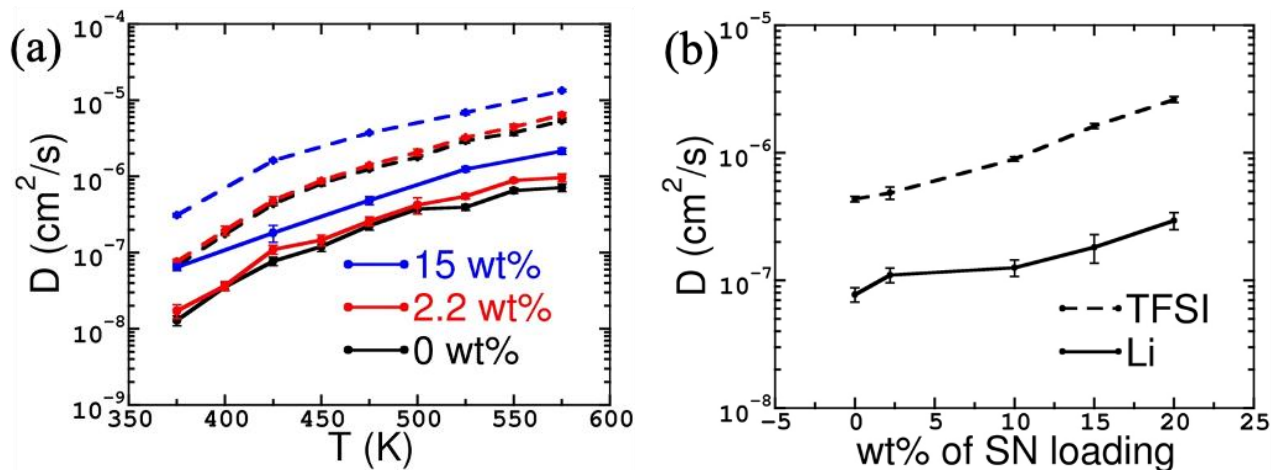


Figure 2. (a) The diffusion coefficient of Li⁺ and TFSI⁻ ions at 0, 2.2, and 15 wt% of SN loadings as a function of temperature, and (b) Diffusion coefficient of Li⁺ and TFSI⁻ ions at 425 K temperature as a function of weight percentage of SN in PEO-LiTFSI electrolytes. The error bar on many data points is too small to be visible and the lines are guide to the eye.

From the MSD results presented in Figure S1, it is observed that the motion of TFSI ion transforms from subdiffusive to the diffusive region after 10⁴ ps. However, the Li ion remains subdiffusive for a relatively longer timescale compared to the diffusive behavior of TFSI ions. Further, the onset of diffusive regimes arrives at a much shorter timescale at higher temperatures. Also, with an increase in temperature both ions move readily towards the diffusive region. Interestingly, we observed that the MSDs for both cation and anion are significantly higher and increased with the loading of SN. Explicitly, we observed that adding SN leads to a faster transformation of the subdiffusive region to a long-time linear diffusive region.

In order to calculate the self-diffusion coefficient correctly from the MD simulations, we used the long-time MSDs. The self-diffusion coefficients of Li and TFSI ions as a function of the temperature at 0, 2.2, and 15 wt% of SN loadings, and also as a function of wt% of SN at 425 K were shown in Figure 2. It follows that the diffusion coefficient increases exponentially with temperature, consistent with the trends observed for MSD curves. Quantitatively, the value D for Li and TFSI ions was found to be 7.7×10^{-8} and 4.3×10^{-7} cm²/s in SN free SPE (i.e., pure PEO melt) which increases to 2.2×10^{-7} and 1.4×10^{-6} cm²/s, respectively when loaded with 20 wt% of SN. It is observed that the diffusion coefficient is found to be higher for TFSI ions than that of Li ions due to the difference in the size of ions. Explicitly, the TFSI ion has a larger size than Li ion which results in a sparsely distributed charge on TFSI ion. Consequently, the TFSI ions interact less with their counter ions and neighbouring positive charge clusters. Further, the Li ions interact strongly with the counterions and negative charge clusters. Therefore, the diffusivity of TFSI is naturally higher than Li ions. Overall, we observed an increase in ion mobility with an increase in the temperature and SN loading.

Qualitatively, the Nernst-Einstein relation suggests that if the ions in SPE are completely uncorrelated, the ionic conductivity of polymer electrolyte increases correspondingly with diffusion coefficients of anion and cation. However, we didn't take our analysis explicitly towards the ionic conductivity, which is beyond the scope of current work. In next section, we focus on explaining the reasons behind the change in diffusivities and understand the mechanisms of ion transport.

3.2. MECHANISMS UNDERLYING ION MOBILITIES

A variety of transport mechanisms are studied both experimentally as well as theoretically for the ion diffusion in polymer electrolytes such as analysing the interaction of Li ion with the counterions and the EO unit of polymer segment by ion hopping.^{14,18,32,54,55} To investigate the reason behind the occurrence of relaxation phenomena contributing towards the ion diffusivity, we studied the ion-pair relaxation by ion-pair autocorrelation function and polymer dynamics by dihedral autocorrelation function. It is understandable that to efficiently transport the ions in polymer electrolytes, the local relaxation and segmental motion of the PEO host are needed.⁵⁶ In spite of many phenomena taking part in ion transport, the ion-pair correlation and polymer segmental mobility were identified as major contributing factors in influencing ion transport.^{13,14,16,18,32-35,57}

To investigate different relaxation phenomena in the simulated SPE systems, we analysed primarily two underlying interactions that may influence the diffusivity of ions. First, the interaction of ions with each other as pair (Li-TFSI) and other, with the polymeric PEO chains. To quantify these, we calculated the ion-pair autocorrelations functions and dihedral autocorrelations functions, respectively.

In principle, we can explain the diffusion phenomenon from the Stokes-Einstein relation as

$$D = \frac{k_B T}{6\pi\eta r}, \text{---(3)}$$

where η is the viscosity, k_B is Boltzmann's constant, T is the temperature, and r is the radius of diffusing particle. In MD simulations, one way to calculate the viscosity from equilibrium simulation is by using the Green-Kubo formula:

$$\eta_{\alpha\beta} = \frac{V}{k_B T} \int_0^{\infty} \langle P_{\alpha\beta}(t_0) P_{\alpha\beta}(t_0 + t) \rangle_{t_0} dt, \text{---(4)}$$

where, V denotes the volume, $P_{\alpha\beta}$ denotes the off-diagonal elements of pressure tensor, $\alpha, \beta = x, y, z$, and $\langle \dots \rangle_{t_0}$ denotes the ensemble average of autocorrelation function over all off-diagonal components and all possible time origins.

However, since the pressure appearing in the above equation fluctuates largely and results in fluctuating long-time tails in the correlation functions,^{58–60} we could not obtain sufficient sampling of the viscosity calculations. Therefore, instead of analysing the diffusion coefficient results directly in terms of viscosity due to statistics, we calculate the underlying relaxation timescales which scales as η/T^{61-63} and is equivalent to using shear viscosity in analysing the diffusion coefficient results.

3.2.1. The Li-TFSI Ion-pair Autocorrelation Functions.

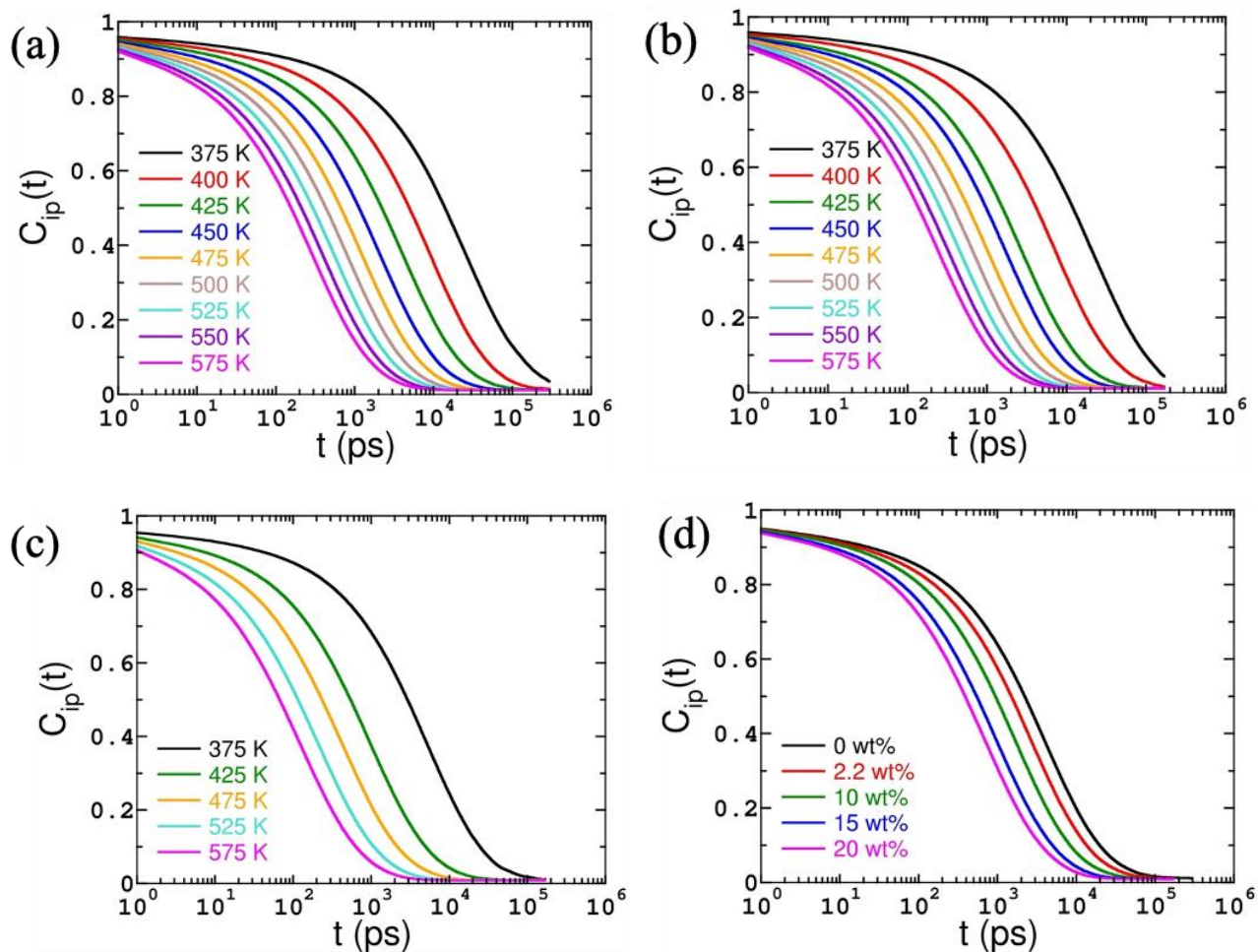


Figure 3: The ion-pair autocorrelation functions of Li-TFSI ion-pairs for (a) 0, (b) 2.2, and (c) 15 wt% of SN loadings at different temperatures, respectively, and (d) The ion-pair autocorrelation functions of Li-TFSI ion-pairs for 425 K at different wt% of SN loadings.

The primary role of SN in the SPE was to influence the diffusivity of ions as discussed in the previous section. It is expected that a higher values of diffusion coefficient of ions will result in significant increase in ionic conductivities. However, the overall diffusivities and ionic conductivities ultimately depend on the cation-anion correlations and the underlying relaxation phenomena. To gain a fundamental understanding of the above, we begin our analysis by asking “what is the role of ion-pair

correlation timescales on ionic diffusivities?” and examine the relationship between the ion-pair relaxation timescales and the ion transport. In simulations, by constructing a population variable to label whether or not a tagged ion-pair is intact, we calculated the ion-pair autocorrelation function $C_{ip}(t)$ as,

$$C_{ip}(t) = \frac{\langle h(t)h(0) \rangle}{\langle h(0)h(0) \rangle}, \quad (5)$$

where, the population variable $h(t)$ is assigned a value 1 when an ion-pair is found intact (i.e., TFSI has a Li^+ in its first coordination shell of 10 \AA , and vice-versa), and 0 otherwise. The angular brackets account for the ensemble averaging of time correlation function over all possible ion-pairs and time origins. To quantify the ion-pair relaxation timescales, we fitted the simulated results for $C_{ip}(t)$ to the Kohlrausch-Williams-Watts (KWW) stretched exponential function of the form $C_{ip}(t) = e^{-\left(\frac{t}{t_{\text{KWW}}}\right)^{\beta_{\text{KWW}}^{ip}}}$, where t_{KWW} and β_{KWW}^{ip} are the fitting parameters.

The $C_{ip}(t)$ basically, tells us the probability that the two pairs Li-TFSI are intact at time t , given that it was intact at time zero. This is calculated from simulated trajectories by observing the joint occurrence of two non-zero populations separated by time t . Therefore, at equilibrium, the probability of having a specific pair bonded in a large system is zero, i.e., $C_{ip}(t) = 0$.⁶⁴ Here, we took a cut-off distance of 10 \AA between the Li-TFSI ionic pairs. Also, $C_{ip}(0) = 1$ indicates that ion-pairs are completely correlated at initial time. The $C_{ip}(t)$ between the pairs Li-TFSI is shown in Figure 3 for different wt% of SN at 425 K and for the different temperatures at 0, 2.2, and 15 wt% of SN loadings. The $C_{ip}(t)$ decays rather slowly reaching approximately 0.90 - 0.95 within 1 ps and to zero on the scale of 10^5 ps. We observed a similar behavior in both cases of temperature variation and wt% variation. Explicitly, we observed that $C_{ip}(t)$ decays rapidly when polymer electrolyte is loaded with SN as compared to pure PEO melt or the temperature, which means that ion aggregation of Li-TFSI pairs is depressed significantly indicating that Li ions are interacting only for a shorter time with TFSI ions.

The ion-pair relaxation time τ_{ip} was calculated as the total area under the curve $C_{ip}(t)$ such that,

$$\tau_{ip} = \int_0^{\infty} C_{ip}(t) dt = \int_0^{\infty} \exp \left[-\left(\frac{t}{t_{\text{KWW}}}\right)^{\beta_{\text{KWW}}^{ip}} \right] dt = t_{\text{KWW}} \Gamma \left(1 + \frac{1}{\beta_{\text{KWW}}^{ip}} \right), \quad (6)$$

where Γ denotes the Gamma function.

The results of τ_{ip} at different SN loadings and wt%s were displayed in Figure 4. We notice that with increase in SN loading and temperature, the ion-pair relaxation time τ_{ip} was found to decrease monotonically. This indicates faster ion-pair relaxations consistent with the $C_{ip}(t)$. Apparently, the rate of change of τ_{ip} is comparable qualitatively with that of the trends observed for D of ionic species.

To gain deeper insights into the role of ion-pair relaxation timescales on the diffusivities, we have plotted the diffusion coefficient as a function of τ_{ip} as shown in Figure 4. The diffusion coefficient is found to decrease with the ion-pair relaxation timescales consistently for all the loadings of SN in the electrolyte. The slower relaxations hinder the motion of both the ions in the electrolyte because the tendency of ion-pairing is more pronounced. Therefore, we observed a higher degree of correlations between the diffusion coefficient of Li and TFSI ions and ion-pair relaxation timescales. Further, to quantify such a behavior, we have analysed the degree of correlations by fitting the diffusion coefficient of ionic species to $D = \alpha_{ip}/\tau_{ip}^{\gamma_{ip}}$ where, γ_{ip} is ion-pair relaxation exponent.

For the lithium and TFSI ions, we find that the degree of correlation is 0.85 and 0.91, respectively. These exponents point out slight deviations from the ideal Stoke-Einstein (SE) behavior that corresponds to an exponent 1 shown as a dashed line in Figure 4. The corresponding parameter when fitted with the ideal SE relation are given as $\alpha = 0.00058$ for Li-ions and $\alpha = 0.0036$ for TFSI ions. The degree of deviation from the ideal Stoke-Einstein behavior is somewhat higher for the Li ions as compared to that of the TFSI ions as noticed in Figures 4(a) and 4(b). The same degree of uncorrelation is quantified by plotting $D\tau_{ip}$ vs τ_{ip} in Figure 5 where the dashed line indicates the ideal Stokes-Einstein relation and the continuous line was drawn to guide the eye. It is now very clear that the degree of uncorrelation is indeed small for TFSI but very high for Li-ions.

Since Li and TFSI ions naturally form ion-pairs with each other, the corresponding relation phenomenon is expected to influence equally the diffusion behavior of both the ion types. However, the deviation is higher for the Li ions and suggests that Li ions are probably influenced by a different transport mechanism that is likely caused by the PEO polymer chains. Further, the results presented in Figures 4 and 5 are conclusively pointing out the underlying deviations from the ideal SE relation which is also confirming the ion-pair relaxation is not yet sufficient for explaining the diffusion coefficient result which is even worse for Li case.

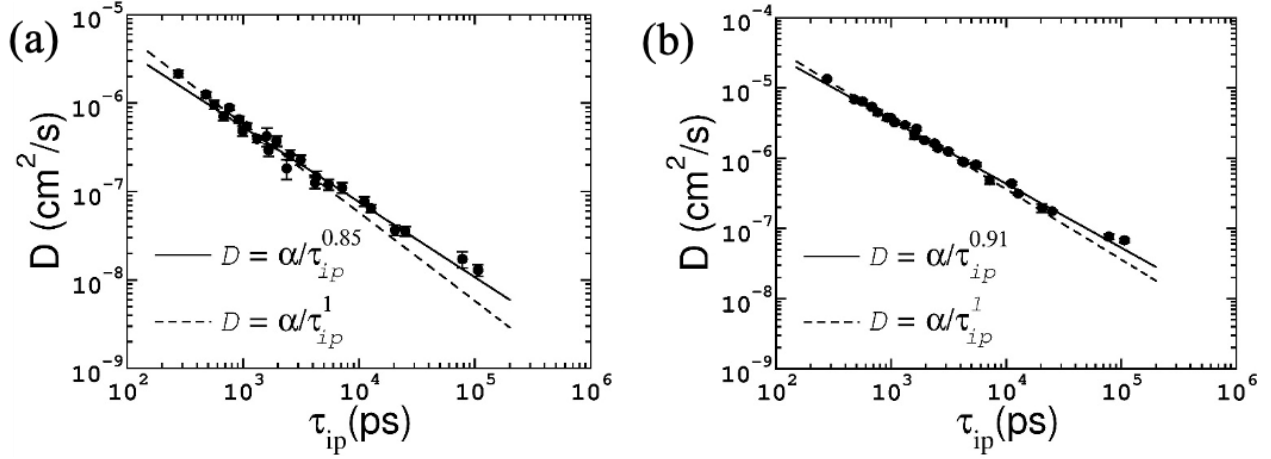


Figure 4: The diffusion coefficient as a function of the ion-pair relaxation time for (a) Li, and (b) TFSI ions. The solid lines represent fitting of the simulation data to eq $D = \alpha_{ip}/\tau_{ip}^{\gamma_{ip}}$, where α and γ_{ip} are fitting parameters, and dashed lines represent fitting of the simulation data to ideal SE behavior with eq $D = \alpha/\tau_{ip}$, where α is a fitting parameter. The fitted α values are: $\alpha = 0.00058$ and 0.0036 for Li and TFSI, respectively when the exponent is fixed at a value 1.

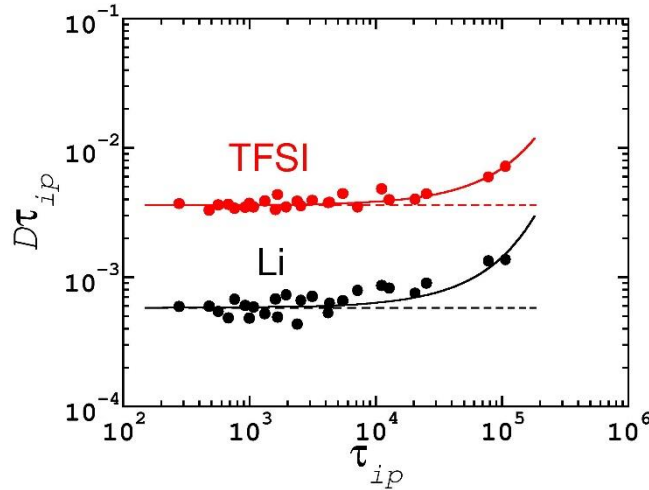


Figure 5: Verification of the deviation from SE relation: comparison of $D\tau_{ip}$ vs τ_{ip} for simulation data of Li and TFSI ions at all temperatures and wt%*s*. The dashed lines represent ideal SE behavior and solid lines are drawn to guide the eye using equations $D\tau_{ip} = 5.8 \times 10^{-4} e^{9.1 \times 10^{-6} \tau_{ip}}$ and $D\tau_{ip} = 3.6 \times 10^{-3} e^{6.6 \times 10^{-6} \tau_{ip}}$, respectively for Li and TFSI ions.

To understand how ionic diffusivities are correlated to the ion-pair relaxation phenomenon when the loading of SN is changed, we further decomposed the data as shown in Figure 6. One of the main questions in this regard is: How does the correlations between diffusivities and relaxation timescales change at different loadings within the case of changing the temperature (Figures 6(a-c)) in the polymer electrolyte?. Further, we seek to understand how differently does the ion-pair relaxation phenomenon influence the ion transport behavior when changing the temperature (Figures 6(a-c)) versus when

changing the loading of SN (Figures 6(d)) in the polymer electrolyte. Not surprisingly, we observed that the decomposed data confirm the same physics that the deviations from ideal SE relation are larger in the case of Li ions but relatively lower in TFSI ions, consistent with the results presented in Figure 4. Interestingly, we observe that the correlations approach towards a one-to-one correspondence scenario at higher loadings of SN for both types of ions indicating smaller deviations from the ideal SE relation at higher loadings. However, the correlations worsen for lithium ions but better for TFSI ions when changing the loading of SN in the polymer electrolyte at 425 K (Figure 6(d)).

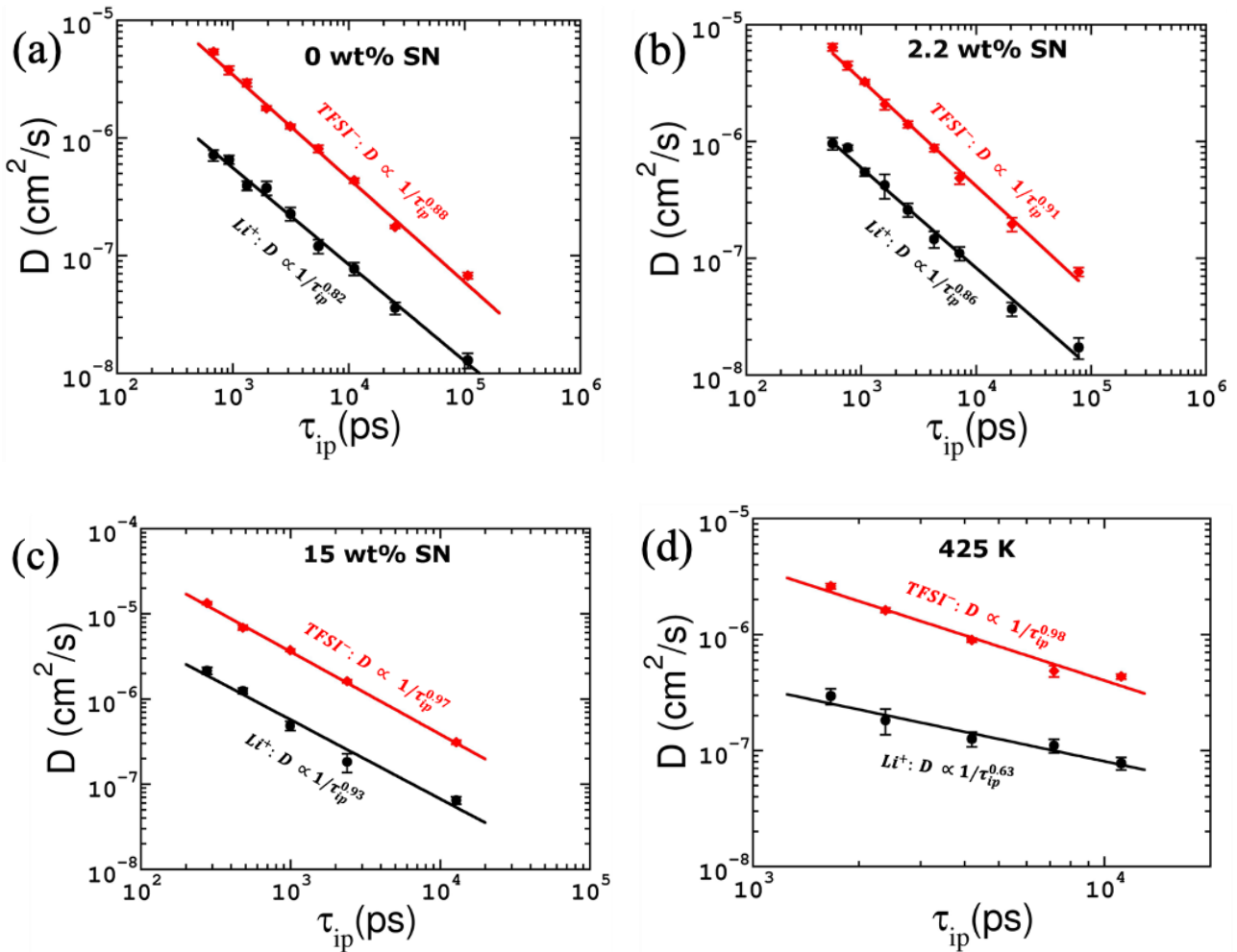


Figure 6: The diffusion coefficient as a function of the ion-pair relaxation time for (a) 0, (b) 2.2, and (c) 15 wt% loadings of SN at different temperatures, and (d) for different loadings at 425 K.

Together, the results presented in Figures 4-6 collectively suggest that the ion diffusivity of both types of ions is only *either partially or poorly* described by the underlying ion-pair relaxation phenomenon in most of the scenarios and *completely* in only two scenarios for the TFSI ions: (i) Temperature induced faster diffusion at a loading of 15 wt% with an exponent of 0.97, and (ii) SN loading induced faster diffusion at 425 K with an exponent of 0.98. The *partial or poor* correlations between ion

transport and underlying ion-pair relaxation phenomenon in the case of lithium ions indicate that the diffusivity of Li-ions may be only described by invoking different other transport mechanisms. The above analysis suggests that no polymer groups interact with TFSI ions favourably to provide ion transport pathways but lithium may have favourable transport pathways along the backbone of polymer segments. Therefore, we further explored the dihedral angle autocorrelation functions because the Li-ion is expected to interact more closely with the polymer chains in contrast to TFSI ions which are only interacting through ion-pair interaction with Li-ions. We, therefore, examine the hypothesis that the interplay of Li-ion interactions with polymer segments is possibly responsible for Li-ion transport in the following section.

3.2.2. Polymer Segmental Motion Through Dihedral Autocorrelation Functions.

As we have discussed in the previous section, the polymer segmental motion of PEO chains, also crucial in understanding ion mobility. Moreover, from the results of the diffusion coefficient, it appears that the effect of SN loading has the same qualitative effect as by the temperature. Since the temperature affects the polymer segmental dynamics, loading of the SN may also affect the polymer dynamics. Therefore, we have examined the polymer dynamics and their correlation with ion mobility/diffusivity.

To understand this behavior, we calculated the dihedral autocorrelation function $C_\phi(t)$ involving C-O-C-C atoms in PEO chains as³²

$$C_\phi(t) = \frac{\langle \cos\phi(t)\cos\phi(0) \rangle - \langle \cos\phi(0) \rangle^2}{\langle \cos\phi(0)\cos\phi(0) \rangle - \langle \cos\phi(0) \rangle^2}, \quad (7)$$

where $\phi(t)$ is the dihedral angle of C-O-C-C atoms in the PEO chain at time t and $\langle \dots \rangle$ represents the ensemble average over all possible C-O-C-C dihedral angles and time origins. By definition, the $C_\phi(0) = 1$ and decays to zero much faster than the ion-pair time correlation function $C_{ip}(t)$. Due to the inherent faster polymer dynamics $C_\phi(t)$ rapidly decays to almost 0.6-0.8 depending on the temperature within just 1 ps, we saved the trajectories with a frequency of 10 fs to capture the fast relaxations. We considered 10 such independent trajectories of high saving frequency and the resulting average $C(t)$ was shown in Figure 7 for lag times up to 1 ps. We observed that there is significant decay in dihedral autocorrelation function $C_\phi(t)$ for different temperatures. However, the $C_\phi(t)$ is not affected by SN at 425 K and remains almost constant till 1 ps for all the wt% and starts decaying slowly as compared to pure PEO.

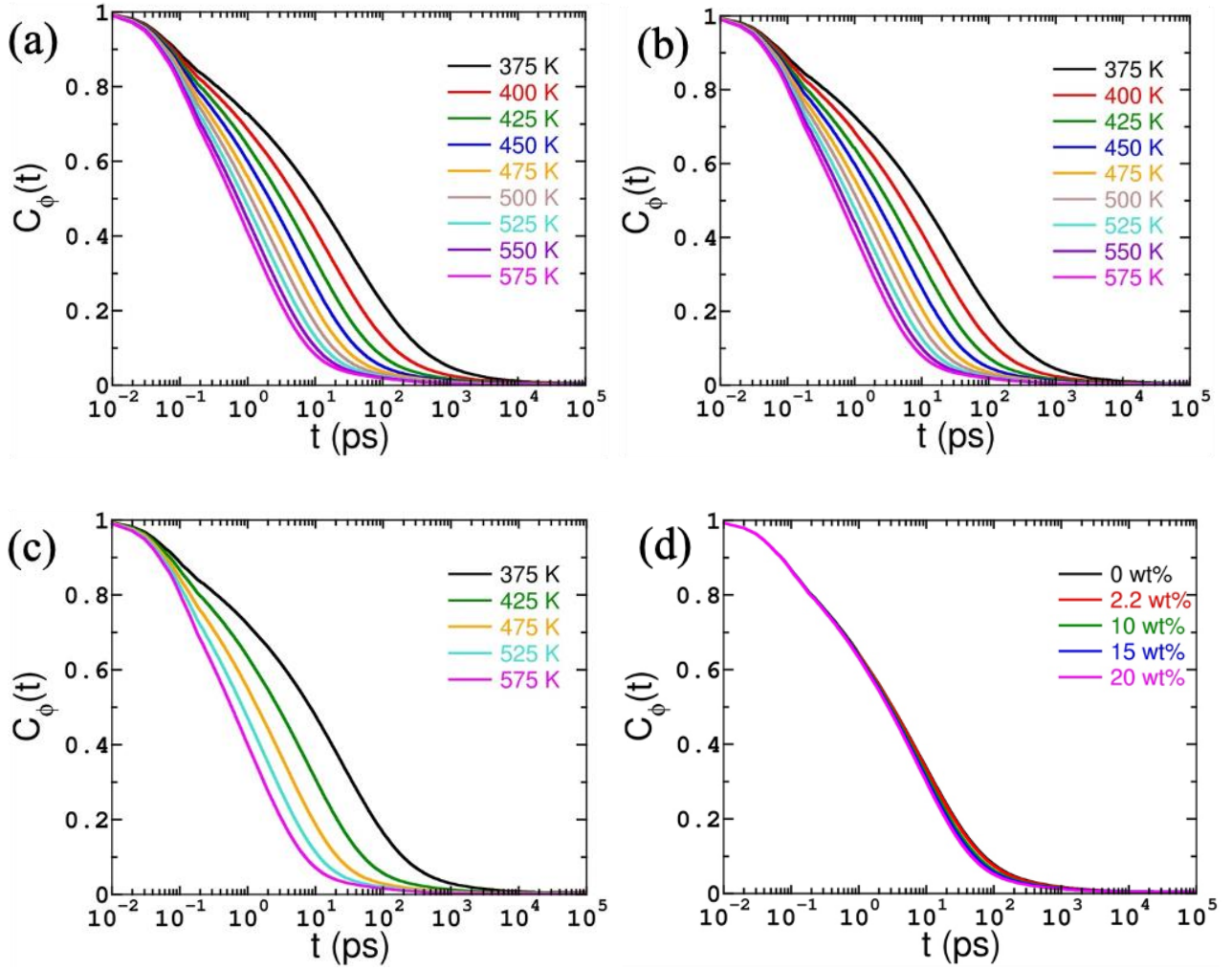


Figure 7. The dihedral angle autocorrelation functions of PEO chains for (a) 0, (b) 2.2, and (c) 15 wt% loadings of SN at different temperatures, and (d) dihedral autocorrelation function for different loadings of SN molecules at 425 K.

The results of $C_\phi(t)$ for different temperatures and loading are shown in Figure 7. We observed that at high temperature there is a sharp decay in $C_\phi(t)$ whereas, with an increase in loading of SN, the $C_\phi(t)$ does not decay significantly as compared to pure PEO melt. Also, by analysing the corresponding polymer relaxation times τ_ϕ , we observed a counter-intuitive behavior of D vs τ_ϕ at different loading of SN. The $C_\phi(t)$ was found to decrease consistently with increasing temperatures. It means PEO chains exhibit faster segmental dynamics with an increase in temperature but the same is not true for a similar increase in wt% of SN. Now, to understand the effect of polymer segmental relaxation on the diffusion of ions, we plotted the corresponding diffusion coefficient of ions with the dihedral angle relaxation time τ_ϕ as shown in Figure 8.

Similar to ion pair autocorrelation function here we have fitted the $C_\phi(t)$ with KWW stretched exponential functions and calculated the dihedral relaxation times as, $\tau_\phi = t_{\text{KWW}}\Gamma\left(1 + \frac{1}{\beta_{\text{KWW}}^\phi}\right)$. We observed τ_ϕ decreases exponentially with the loading of SN in the system which indicates the presence of SN makes the polymer more dynamic which indirectly is expected to help in faster transport of ions. Similarly, τ_ϕ also decreases significantly with the increase in temperature. Qualitatively, the behavior is like an Arrhenius indicating that there could be correlations between the diffusion coefficient and dihedral angle relaxation timescales. To quantify the degree of correlation between the D and dihedral angle relaxation time, we fitted D vs τ_ϕ with the equation $D = \alpha/\tau_\phi^{\gamma_\phi}$ and obtained the fitting parameter α and exponent γ_ϕ as shown in Figure 8 for all wt%^s and temperatures. Interestingly, we observed that the diffusion coefficient of Li correlates excellently with dihedral angle relaxation timescales but for TFSI ions, a slight deviation is observed with exponent close to 1.0.

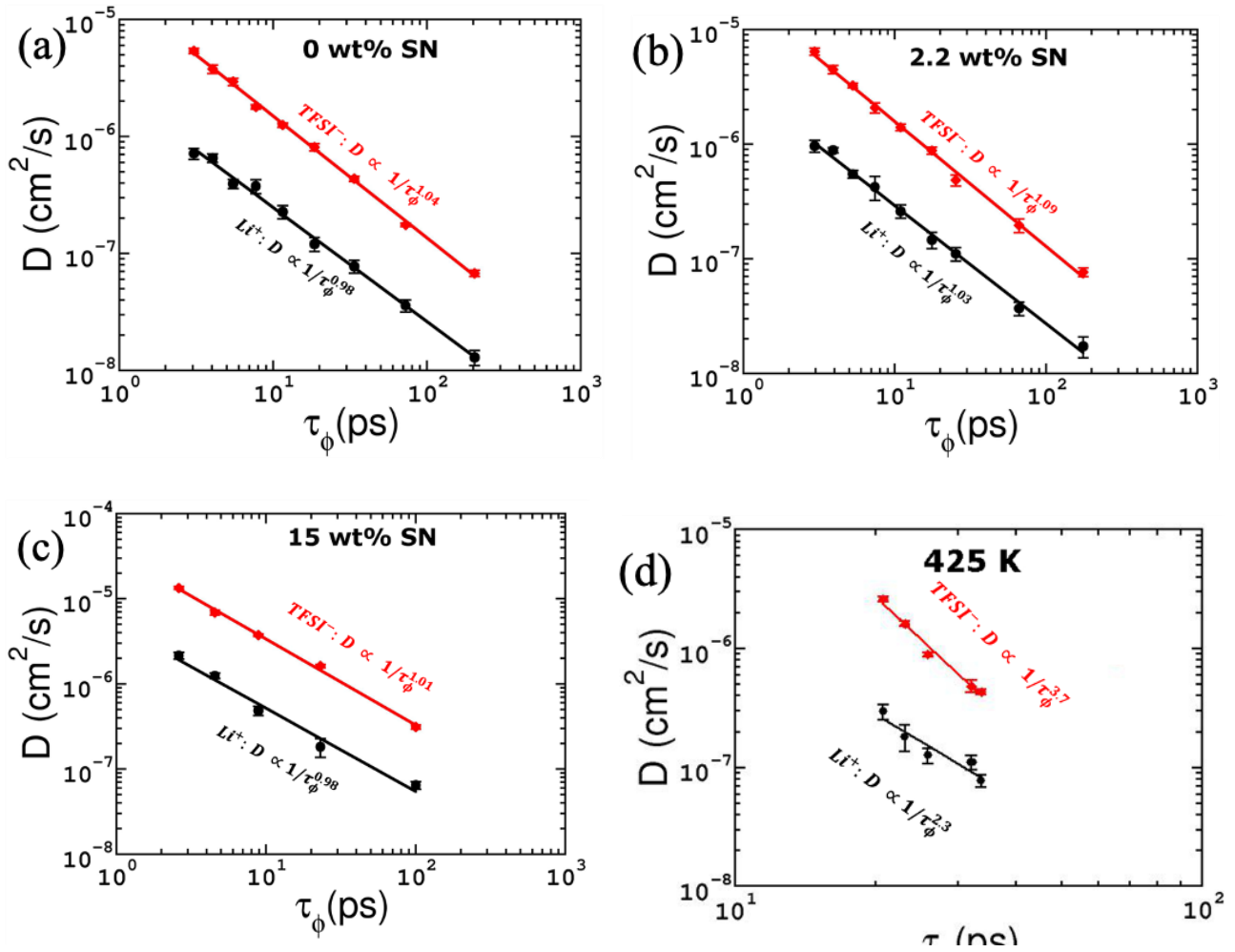


Figure 8: The diffusion coefficient as a function of the dihedral angle relaxation time for (a) 0, (b) 2.2, and (c) 15 wt%^s loadings of SN at different temperatures, and (d) for different loadings at 425 K.

We observed that the exponent γ for Li^+ ion and TFSI^- ion for both the analysis done with different wt% of SN at 425 K and different temperatures at 0, 2.2, 15 wt% of loading of SN, respectively. Earlier, we found that there is an ambiguity in understanding the Li^+ mobility from ion-pair relaxation. Therefore, we hypothesized that the dihedral angle relaxation timescales might be able to succeed in explaining this. Considering temperature effects at 2.2 wt% of SN for Li^+ ion the value of the exponent is increased from 0.82 to 0.98 confirming our hypothesis that Li^+ ions are getting transported more with the segmental motion of PEO chains rather than ion-pairing. But for loading effects, the exponents for Li^+ comes out to be counterintuitive as it increased from 0.63 to 2.3 which is completely deviated from what we have expected. A similar observation is made for the TFSI ions as well for the case of SN loading induced changes in diffusion coefficient.

So, together the direct/indirect influence of SN on polymer relaxation timescales or ion pair relaxation timescales are not directly useful in explain the diffusivity of Li ions completely. This is a surprising result where the transport mechanism associated with Li ions are more complex than ion pair relaxation timescales and polymer segmental motion. Further investigation is required to completely establish this phenomenon. This means that there left some other mechanism that defines the diffusivity of Li^+ ions when loaded with SN.

4. CONCLUSIONS

To summarize, atomistic molecular dynamics simulations were performed to study the effect of loading of SN on the diffusivity of ionic species in PEO-LiTFSI electrolytes and to understand the underlying transport mechanisms in the solid polymer electrolyte. A sufficient number of SN molecules were dispersed to prepare succinonitrile weight percentages of 0, 2.2, 10, 15, and 20 in the PEO melt along with dissolved LiTFSI salt at a specific salt concentration ratio of EO:Li=12.5:1. The temperature effects were also studied at selected loading of 0, 2.2, and 15 wt% of SN in the range between 375 – 575 K. To describe the interactions between different molecular species at the atomistic level, we employed the optimized potentials for liquid simulations (OPLS) force field parameters developed by Jorgensen group.³⁸

The simulations were performed with GROMACS simulation package³⁷ in NPT ensemble⁶⁵ and 350 ns long production trajectories were generated at each temperature for 0 wt% and 200 ns for other systems. The length of the trajectories was found to be sufficient to sample the diffusive regime of the mean-squared displacements and the long-time relaxation behavior of ion-pair correlation functions. Since the long trajectories were saved at a frequency of 1 ps, we observed a serious lack of fast relaxation phenomena contribution while examining the polymer segmental dynamics. Therefore, to

capture the relaxation phenomena associated with higher resolution in timescales, in our simulations, we generated 10 independent trajectories of each 1 ns length with a saving frequency of 10 fs. The completely uncorrelated microstates with different initial positions and momenta are considered for such simulations which were taken along the production trajectories at regular intervals.

The diffusion coefficient of ionic species was calculated from the long-time diffusive regime of the mean-squared displacements and examined the fundamental origin of ion transport in the SN loaded solid polymer electrolytes by invoking the underlying relaxation phenomena. We find that the diffusivity of both cation and anion increases monotonically with the loading of SN and also with an increase in temperature. The diffusion coefficient of TFSI ions was found to be higher than that of the lithium ions at a given temperature and loading of SN molecules. These results offer an interesting future promise for the use of succinonitrile as a plasticizer to increase the ionic transport characteristics of PEO-based solid polymer electrolytes.

To explain the mechanisms behind increased diffusion of ionic species, we analysed different relaxation timescales associated with the Li-TFSI ion-pair dynamics and polymer segmental dynamics by calculating the respective ion-pair autocorrelation functions and dihedral angle autocorrelation functions. We computed the ion-pair and polymer segmental relaxation timescales by fitting the respective autocorrelation functions to Kohlrausch–Williams–Watts (KWW) stretched exponential functions. We observed both τ_{ip} and τ_{ϕ} to decrease monotonically with an increase in the loading of SN and temperature revealing accelerated relaxation behavior of SN-PEO-LiTFSI electrolytes. We further investigated the inherent connection between the ion-pair relaxation timescales, polymer segmental timescales, and ionic diffusivities and found that both the relaxation timescales are necessary to completely explain the diffusivities of ions. While the TFSI ions are found to diffuse in the electrolytes by the influence of primarily the ion-pair interactions, the diffusion mechanism of lithium ions is strongly affected by the interactions of Li ions coming from both the TFSI ions and the PEO polymer chains. However, the analysis of correlations between diffusion coefficient of ions as a function of wt% of SN loading and different timescales point out unusual SN-induced transport mechanisms in SN-PEO-LiTFSI electrolytes.

Overall, our simulations suggest that SN molecules have a strong effect on the Li⁺ ion mobility in poly(ethylene oxide) with dissolved Li-TFSI polymer electrolytes and may boost the choice of PEO-based solid polymer electrolytes possessing higher ionic conductivity for commercial applications. Our deeper analysis led to an interesting question for future investigations that ion transport in SN-loaded electrolytes cannot be completely described by ion-pairing behavior and polymer segmental

motion of PEO chains and that existence of interplay between other distinct transport mechanisms influencing ion transport.

AUTHOR INFORMATION

Corresponding Author

*E-mail: santosh@iitj.ac.in

Notes

The authors declare no competing financial interest.

ACKNOWLEDGMENTS

The authors acknowledge the Computer Center of IIT Jodhpur for providing computing resources that have contributed to the research results reported within this paper. The authors acknowledge stimulating discussions with Prabhat K Jaiswal and Ananya Debnath.

REFERENCES

- (1) Cardini, G.; Righini, R.; Califano, S. Computer Simulation of the Dynamics of the Plastic Phase of Succinonitrile. *The Journal of Chemical Physics* **1991**, *95* (1), 679–685. <https://doi.org/10.1063/1.461418>.
- (2) Tarascon, J.-M.; Armand, M. Issues and Challenges Facing Rechargeable Lithium Batteries. *Nature* **2001**, *414* (6861), 359–367. <https://doi.org/10.1038/35104644>.
- (3) Goodenough, J. B.; Park, K.-S. The Li-Ion Rechargeable Battery: A Perspective. *Journal of the American Chemical Society* **2013**, *135* (4), 1167–1176. <https://doi.org/10.1021/JA3091438>.
- (4) Manthiram, A.; Yu, X.; Wang, S. Lithium Battery Chemistries Enabled by Solid-State Electrolytes. *Nature Reviews Materials* **2017**, *2* (4), 1–16. <https://doi.org/10.1038/natrevmats.2016.103>.
- (5) Xia, S.; Wu, X.; Zhang, Z.; Cui, Y.; Liu, W. Practical Challenges and Future Perspectives of All-Solid-State Lithium-Metal Batteries. *Chem* **2019**, *5* (4), 753–785. <https://doi.org/10.1016/J.CHEMPR.2018.11.013>.
- (6) Qiu, J.; Liu, X.; Chen, R.; Li, Q.; Wang, Y.; Chen, P.; Gan, L.; Lee, S.-J.; Nordlund, D.; Liu, Y.; Yu, X.; Bai, X.; Li, H.; Chen, L. Enabling Stable Cycling of 4.2 V High-Voltage All-Solid-State Batteries with PEO-Based Solid Electrolyte. *Advanced Functional Materials* **2020**, *30* (22), 1909392. <https://doi.org/10.1002/ADFM.201909392>.
- (7) Armand, M. B.; Bruce, P. G.; Forsyth, M.; Scrosati, B.; Wiczczonek, W. Polymer Electrolytes. *Energy Materials* **2011**, 1–31. <https://doi.org/10.1002/9780470977798.CH1>.
- (8) Xue, Z.; He, D.; Xie, X. Poly(Ethylene Oxide)-Based Electrolytes for Lithium-Ion Batteries. *Journal of Materials Chemistry A* **2015**, *3* (38), 19218–19253. <https://doi.org/10.1039/C5TA03471J>.
- (9) Fenton, D. E.; Parker, J. M.; Wright, P. v. Complexes of Alkali Metal Ions with Poly(Ethylene Oxide). *Polymer* **1973**, *14* (11), 589. [https://doi.org/10.1016/0032-3861\(73\)90146-8](https://doi.org/10.1016/0032-3861(73)90146-8).

- (10) Wright, P. v. Electrical Conductivity in Ionic Complexes of Poly(Ethylene Oxide). *British Polymer Journal* **1975**, 7 (5), 319–327. <https://doi.org/10.1002/PL4980070505>.
- (11) Vashishta, P.; Mundy, J. N.; Shenoy, G. K. Fast Ion Transport in Solids : Electrodes, and Electrolytes : Proceedings of the International Conference on Fast Ion Transport in Solids, Electrodes, and Electrolytes, Lake Geneva, Wisconsin, U.S.A., May 21-25, 1979. **1979**, 744.
- (12) Armand, M. Polymer Solid Electrolytes - an Overview. *Solid State Ionics* **1983**, 9–10 (PART 2), 745–754. [https://doi.org/10.1016/0167-2738\(83\)90083-8](https://doi.org/10.1016/0167-2738(83)90083-8).
- (13) Borodin, O.; Smith, G. D. Molecular Dynamics Simulation Study of Lii-Doped Diglyme and Poly(Ethylene Oxide) Solutions. *Journal of Physical Chemistry B* **2000**, 104 (33), 8017–8022. <https://doi.org/10.1021/jp0011443>.
- (14) Borodin, O.; Smith, G. D. Mechanism of Ion Transport in Amorphous Poly(Ethylene Oxide)/ LiTFSI from Molecular Dynamics Simulations. *Macromolecules* **2006**, 39 (4), 1620–1629. <https://doi.org/10.1021/ma052277v>.
- (15) Diddens, D.; Heuer, A.; Borodin, O. Understanding the Lithium Transport within a Rouse-Based Model for a PEO/LiTFSI Polymer Electrolyte. *Macromolecules* **2010**, 43 (4), 2028–2036. <https://doi.org/10.1021/ma901893h>.
- (16) Mogurampelly, S.; Borodin, O.; Ganesan, V. Computer Simulations of Ion Transport in Polymer Electrolyte Membranes. <http://dx.doi.org/10.1146/annurev-chembioeng-080615-034655> **2016**, 7, 349–371. <https://doi.org/10.1146/ANNUREV-CHEMBIOENG-080615-034655>.
- (17) Hu, J. J.; Long, G. K.; Liu, S.; Li, G. R.; Gao, X. P. A LiFSI–LiTFSI Binary-Salt Electrolyte to Achieve High Capacity and Cycle Stability for a Li–S Battery. *Chemical Communications* **2014**, 50 (93), 14647–14650. <https://doi.org/10.1039/c4cc06666a>.
- (18) Molinari, N.; Mailoa, J. P.; Kozinsky, B. Effect of Salt Concentration on Ion Clustering and Transport in Polymer Solid Electrolytes: A Molecular Dynamics Study of PEO-LiTFSI. *Chemistry of Materials* **2018**, 30 (18), 6298–6306. <https://doi.org/10.1021/acs.chemmater.8b01955>.
- (19) Kubisiak, P.; Wróbel, P.; Eilmes, A. Molecular Dynamics Investigation of Correlations in Ion Transport in MeTFSI/EMIM-TFSI (Me = Li, Na) Electrolytes. *Journal of Physical Chemistry B* **2020**, 124 (2), 413–421. <https://doi.org/10.1021/acs.jpccb.9b10391>.
- (20) Nti, F.; Greene, G. W.; Zhu, H.; Howlett, P. C.; Forsyth, M.; Wang, X. Anion Effects on the Properties of OIPC/PVDF Composites. *Materials Advances* **2021**, 2 (5), 1683–1694. <https://doi.org/10.1039/d0ma00992j>.
- (21) Kim, Y. T.; Smotkin, E. S. The Effect of Plasticizers on Transport and Electrochemical Properties of PEO-Based Electrolytes for Lithium Rechargeable Batteries. *Solid State Ionics* **2002**, 149 (1–2), 29–37. [https://doi.org/10.1016/S0167-2738\(02\)00130-3](https://doi.org/10.1016/S0167-2738(02)00130-3).
- (22) Neyertz, S.; Brown, D. Local Structure and Mobility of Ions in Polymer Electrolytes: A Molecular Dynamics Simulation Study of the Amorphous PEOxNaI System. *Journal of Chemical Physics* **1996**, 104 (10), 3797–3809. <https://doi.org/10.1063/1.471033>.
- (23) Borodin, O.; Smith, G. D. Molecular Dynamics Simulations of Poly(Ethylene Oxide)/LiI Melts. 2. Dynamic Properties. *Macromolecules* **2000**, 33 (6), 2273–2283. <https://doi.org/10.1021/ma991429h>.
- (24) Kasemägi, H.; Klintonberg, M.; Aabloo, A.; Thomas, J. O. Molecular Dynamics Simulation of the LiBF₄-PEO System Containing Al₂O₃ Nanoparticles. *Solid State Ionics* **2002**, 147 (3–4), 367–375. [https://doi.org/10.1016/S0167-2738\(02\)00013-9](https://doi.org/10.1016/S0167-2738(02)00013-9).

- (25) Wu, H.; Wick, C. D. Computational Investigation on the Role of Plasticizers on Ion Conductivity in Poly(Ethylene Oxide) LiTFSI Electrolytes. *Macromolecules* **2010**, *43* (7), 3502–3510. <https://doi.org/10.1021/ma902758w>.
- (26) Diddens, D.; Heuer, A. Lithium Ion Transport Mechanism in Ternary Polymer Electrolyte-Ionic Liquid Mixtures: A Molecular Dynamics Simulation Study. *ACS Macro Letters* **2013**, *2* (4), 322–326. <https://doi.org/10.1021/mz3006457>.
- (27) Das, S.; Ghosh, A. Effect of Plasticizers on Ionic Conductivity and Dielectric Relaxation of PEO-LiClO₄ Polymer Electrolyte. *Electrochimica Acta* **2015**, *171*, 59–65. <https://doi.org/10.1016/j.electacta.2015.04.178>.
- (28) Fan, L. Z.; Maier, J. Composite Effects in Poly(Ethylene Oxide)-Succinonitrile Based All-Solid Electrolytes. *Electrochemistry Communications* **2006**, *8* (11), 1753–1756. <https://doi.org/10.1016/j.elecom.2006.08.017>.
- (29) Whitfield, P. S.; le Page, Y.; Abouimrane, A.; Davidson, I. J. Ab Initio Structure Determination of the Low-Temperature Phase of Succinonitrile from Laboratory X-Ray Powder Diffraction Data—Coping with Potential Poor Powder Quality Using DFT Ab Initio Methods. *Powder Diffraction* **2008**, *23* (4), 292–299. <https://doi.org/10.1154/1.3009635>.
- (30) Zachariah, M.; Romanini, M.; Tripathi, P.; Barrio, M.; Tamarit, J. L.; Macovez, R. Self-Diffusion, Phase Behavior, and Li⁺ Ion Conduction in Succinonitrile-Based Plastic Cocrystals. *Journal of Physical Chemistry C* **2015**, *119* (49), 27298–27306. <https://doi.org/10.1021/acs.jpcc.5b09380>.
- (31) Villarreal, J.; Chavez, R. O.; Chopade, S. A.; Lodge, T. P.; Alcoutlabi, M. The Use of Succinonitrile as an Electrolyte Additive for Composite-Fiber Membranes in Lithium-Ion Batteries. *Membranes* **2020**, *10* (3), 45. <https://doi.org/10.3390/MEMBRANES10030045>.
- (32) Mogurampelly, S.; Ganesan, V. Effect of Nanoparticles on Ion Transport in Polymer Electrolytes. *Macromolecules* **2015**, *48* (8), 2773–2786. <https://doi.org/10.1021/ma502578s>.
- (33) Mogurampelly, S.; Sethuraman, V.; Pryamitsyn, V.; Ganesan, V. Influence of Nanoparticle-Ion and Nanoparticle-Polymer Interactions on Ion Transport and Viscoelastic Properties of Polymer Electrolytes. *The Journal of Chemical Physics* **2016**, *144* (15), 154905. <https://doi.org/10.1063/1.4946047>.
- (34) Mogurampelly, S.; Keith, J. R.; Ganesan, V. Mechanisms Underlying Ion Transport in Polymerized Ionic Liquids. *Journal of the American Chemical Society* **2017**, *139* (28), 9511–9514. <https://doi.org/10.1021/jacs.7b05579>.
- (35) Keith, J. R.; Mogurampelly, S.; Aldukhi, F.; Wheatle, B. K.; Ganesan, V. Influence of Molecular Weight on Ion-Transport Properties of Polymeric Ionic Liquids. *Physical Chemistry Chemical Physics* **2017**, *19* (43), 29134–29145. <https://doi.org/10.1039/c7cp05489k>.
- (36) France-Lanord, A.; Grossman, J. C. Correlations from Ion Pairing and the Nernst-Einstein Equation. *Physical Review Letters* **2019**, *122* (13). <https://doi.org/10.1103/PhysRevLett.122.136001>.
- (37) Berendsen, H. J. C.; van der Spoel, D.; van Drunen, R. GROMACS: A Message-Passing Parallel Molecular Dynamics Implementation. *Computer Physics Communications* **1995**, *91* (1–3), 43–56. [https://doi.org/10.1016/0010-4655\(95\)00042-E](https://doi.org/10.1016/0010-4655(95)00042-E).
- (38) William L. Jorgensen, *; David S. Maxwell, and; Tirado-Rives, J. Development and Testing of the OPLS All-Atom Force Field on Conformational Energetics and Properties of Organic Liquids. *Journal of the American Chemical Society* **1996**, *118* (45), 11225–11236. <https://doi.org/10.1021/JA9621760>.

- (39) Sambasivarao, S. v.; Acevedo, O. Development of OPLS-AA Force Field Parameters for 68 Unique Ionic Liquids. *Journal of Chemical Theory and Computation* **2009**, *5* (4), 1038–1050. <https://doi.org/10.1021/ct900009a>.
- (40) Leontyev, I.; Stuchebrukhov, A. Accounting for Electronic Polarization in Non-Polarizable Force Fields. *Physical Chemistry Chemical Physics* **2011**, *13* (7), 2613–2626. <https://doi.org/10.1039/C0CP01971B>.
- (41) Chaban, V. Polarizability versus Mobility: Atomistic Force Field for Ionic Liquids. *Physical Chemistry Chemical Physics* **2011**, *13* (35), 16055–16062. <https://doi.org/10.1039/C1CP21379B>.
- (42) Chaban, V. v.; Voroshylova, I. v.; Kalugin, O. N. A New Force Field Model for the Simulation of Transport Properties of Imidazolium-Based Ionic Liquids. *Physical Chemistry Chemical Physics* **2011**, *13* (17), 7910–7920. <https://doi.org/10.1039/C0CP02778B>.
- (43) Mogurampelly, S.; Ganesan, V. Structure and Mechanisms Underlying Ion Transport in Ternary Polymer Electrolytes Containing Ionic Liquids. *The Journal of Chemical Physics* **2017**, *146* (7), 074902. <https://doi.org/10.1063/1.4976131>.
- (44) Bhargava, B. L.; Balasubramanian, S. Refined Potential Model for Atomistic Simulations of Ionic Liquid [Bmim][PF₆]. *The Journal of Chemical Physics* **2007**, *127* (11), 114510. <https://doi.org/10.1063/1.2772268>.
- (45) Mondal, A.; Balasubramanian, S. Quantitative Prediction of Physical Properties of Imidazolium Based Room Temperature Ionic Liquids through Determination of Condensed Phase Site Charges: A Refined Force Field. *Journal of Physical Chemistry B* **2014**, *118* (12), 3409–3422. https://doi.org/10.1021/JP500296X/SUPPL_FILE/JP500296X_SI_001.PDF.
- (46) JM, M.; L, M. Packing Optimization for Automated Generation of Complex System's Initial Configurations for Molecular Dynamics and Docking. *Journal of computational chemistry* **2003**, *24* (7), 819–825. <https://doi.org/10.1002/JCC.10216>.
- (47) Martinez, L.; Andrade, R.; Birgin, E. G.; Martínez, J. M. PACKMOL: A Package for Building Initial Configurations for Molecular Dynamics Simulations. *Journal of Computational Chemistry* **2009**, *30* (13), 2157–2164. <https://doi.org/10.1002/jcc.21224>.
- (48) Berendsen, H. J. C.; Postma, J. P. M.; van Gunsteren, W. F.; Dinola, A.; Haak, J. R. Molecular Dynamics with Coupling to an External Bath. *The Journal of Chemical Physics* **1998**, *81* (8), 3684. <https://doi.org/10.1063/1.448118>.
- (49) Nosé, S.; Klein, M. L. Constant Pressure Molecular Dynamics for Molecular Systems. *Molecular Physics* **1983**, *50* (5), 1055–1076. <https://doi.org/10.1080/00268978300102851>.
- (50) Nosé, S.; Nosé; Shūichi. A Molecular Dynamics Method for Simulations in the Canonical Ensemble. *MolPh* **1984**, *52* (2), 255–268. <https://doi.org/10.1080/00268978400101201>.
- (51) Hoover, W. G. Canonical Dynamics: Equilibrium Phase-Space Distributions. *Physical Review A* **1985**, *31* (3), 1695. <https://doi.org/10.1103/PhysRevA.31.1695>.
- (52) Parrinello, M.; Rahman, A. Polymorphic Transitions in Single Crystals: A New Molecular Dynamics Method. *Journal of Applied Physics* **1998**, *52* (12), 7182. <https://doi.org/10.1063/1.328693>.
- (53) Essmann, U.; Perera, L.; Berkowitz, M. L.; Darden, T.; Lee, H.; Pedersen, L. G. A Smooth Particle Mesh Ewald Method. *The Journal of Chemical Physics* **1998**, *103* (19), 8577. <https://doi.org/10.1063/1.470117>.

- (54) Borodin, O.; Smith, G. D. Development of Quantum Chemistry-Based Force Fields for Poly(Ethylene Oxide) with Many-Body Polarization Interactions. *Journal of Physical Chemistry B* **2003**, *107* (28), 6801–6812. <https://doi.org/10.1021/jp027537e>.
- (55) Hanson, B.; Pryamitsyn, V.; Ganesan, V. Mechanisms Underlying Ionic Mobilities in Nanocomposite Polymer Electrolytes. *ACS Macro Letters* **2013**, *2* (11), 1001–1005. <https://doi.org/10.1021/mz400234m>.
- (56) Frech, R.; Chintapalli, S.; Bruce, P. G.; Vincent, C. A. Structure of an Amorphous Polymer Electrolyte, Poly(Ethylene Oxide)₃:LiCF₃SO₃. *Chemical Communications* **1997**, No. 2, 157–158. <https://doi.org/10.1039/a606264d>.
- (57) Gudla, H.; Shao, Y.; Phunnarungsi, S.; Brandell, D.; Zhang, C. Importance of the Ion-Pair Lifetime in Polymer Electrolytes. *The Journal of Physical Chemistry Letters* **2021**, *12* (35), 8460–8464. <https://doi.org/10.1021/ACS.JPCLETT.1C02474>.
- (58) Ernst, M. H.; Hauge, E. H.; Leeuwen, J. M. J. van. Asymptotic Time Behavior of Correlation Functions. *Physical Review Letters* **1970**, *25* (18), 1254. <https://doi.org/10.1103/PhysRevLett.25.1254>.
- (59) Dorfman, J. R.; Cohen, E. G. D. Velocity Correlation Functions in Two and Three Dimensions. *Physical Review Letters* **1970**, *25* (18), 1257. <https://doi.org/10.1103/PhysRevLett.25.1257>.
- (60) Hess, B. Determining the Shear Viscosity of Model Liquids from Molecular Dynamics Simulations. *Journal of Chemical Physics* **2002**, *116* (1), 209–217. <https://doi.org/10.1063/1.1421362>.
- (61) Mezei, F.; Knaak, W.; Farago, B. Neutron Spin Echo Study of Dynamic Correlations near the Liquid-Glass Transition. *Physical Review Letters* **1987**, *58* (6), 571. <https://doi.org/10.1103/PhysRevLett.58.571>.
- (62) Yamamoto, R.; Onuki, A. Heterogeneous Diffusion in Highly Supercooled Liquids. *Physical Review Letters* **1998**, *81* (22), 4915. <https://doi.org/10.1103/PhysRevLett.81.4915>.
- (63) Sengupta, S.; Karmakar, S.; Dasgupta, C.; Sastry, S. Breakdown of the Stokes-Einstein Relation in Two, Three, and Four Dimensions. *The Journal of Chemical Physics* **2013**, *138* (12), 12A548. <https://doi.org/10.1063/1.4792356>.
- (64) Luzar, A.; Chandler, D. Hydrogen-Bond Kinetics in Liquid Water. *Nature* **1996**, *379*:6560–6560, 379 (6560), 55–57. <https://doi.org/10.1038/379055a0>.
- (65) Evans, D. J.; Holian, B. L. The Nose–Hoover Thermostat. *The Journal of Chemical Physics* **1998**, *83* (8), 4069. <https://doi.org/10.1063/1.449071>.